MAXI: Monitor of All-sky X-ray Image

Tatehiro Mihara, Hiroshi Tsunemi, Hitoshi Negoro

1 MAXI mission

Monitor of All-sky X-ray Image (MAXI) is a Japanese X-ray all-sky monitor onboard the International Space Station (ISS). We describe MAXI mission by adopting explanation from [1].

The overview of MAXI is shown in Figure 1. MAXI science instruments consist of two types of X-ray cameras, the Gas Slit Camera (GSC: [2] [3])) and the Solid-state Slit Camera (SSC: [4] [5]). Both GSC and SSC employ slit and collimator optics. Their characteristics are listed in Table 1. The support instruments consist of a Visual Star Camera (VSC) for a precise attitude determination, a Ring Laser Gyroscope (RLG) for a continuous tracking of the attitude, a Global Positioning System (GPS) for an absolute timing and a Loop Heat Pipe and Radiation System (LHPRS). The VSC and the RLG determine the directions of the GSC and the SSC as precisely as a few arc-minutes every second. The LHPRS is used to cool down the SSC camera body which is the hot side of the Peltier cooler of the CCD chip.

The MAXI payload was launched by the space shuttle Endevour on 2009 July 16, then mounted on the port No. 1 on JEM-EF. MAXI started nominal observation since 2009 August 15. The data are publically available from http://maxi.riken.jp.

ISS rotates by itself synchronously with its orbital motion so that one side always faces towards the center of the Earth. Therefore, the sky side of JEM-EF has no Earth occultation of the field of view and surveys a great circle every ISS orbit. MAXI has two Field of Views (FOVs). One is towards the moving-direction (horizon), and the other is towards zenith. The horizontal GSC cameras face a little upwards

Tatehiro Mihara

RIKEN, Wako, Saitama, Japan 351-0198 e-mail: tmihara@riken.jp

Hiroshi Tsunemi

Osaka University, Toyonaka, Osaka Japan 560-0043 e-mail: tsunemi@ess.sci.osaka-u.ac.jp

Hitoshi Negoro

Nihon University, Tokyo, Japan 101-8308 e-mail: negoro.hitoshi@nihon-u.ac.jp

2 Negoro

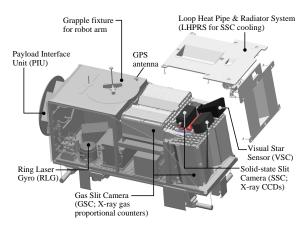


Fig. 1 MAXI overview. MAXI total weight: 520 kg.

away from the horizon by 6 degrees to avoid the Earth rim for any possible ISS attitude. For SSC, the upward angle is 20 degrees to avoid ionized oxygen line from the upper atmosphere. Although a considerably wide FOV is available, the ISS structure, moving solar paddles, docked space-shuttle and Space X vehicle partially block the view of JEM-EF.

The MAXI proposal was finally accepted in 1997 by the National Development Space Agency of Japan (NASDA), now known as the Japan Aerospace Exploration Agency (JAXA). MAXI is the first astronomical payload for JEM-EF on the ISS. Although the launch was scheduled for 2003, the space shuttle, Columbia accident, and the ISS construction delay resulted in the postponement of the MAXI launch to 2009.

A specific object is observed by MAXI with a slit camera for a limited time with every ISS orbit. The X-ray detector of the camera is sensitive to a one dimensional image through the slit, where the rectangular wide FOV through the slit spans the sky perpendicular to the ISS moving direction as shown in Figure 2 in case of GSC $(\pm 1.5^{\circ} \times \pm 40^{\circ})$. The scanning image of an object is obtained with the triangular response of a slat collimator according to ISS rotation. Combination of the slit image and the triangular transmission image makes a source image in the sky, called as a Point Spread Function (PSF) (Figure 3). One-side of PSF is determined by the slats-collimator $(1.5^{\circ}$ for all energies), while the other side of PSF is determined by the position detection capability of the proportional counter (large in low energies, and small for high energies with a tail for a slant incident angle in high energies).

Table 1 Specification of MAXI slit cameras

	GSC†: Gas Slit Camera	SSC†: Solid-state Slit Camera
X-ray detector	12 pieces of one- dimensional PSPC; Xe 99 % + CO ₂ 1 %, 1.4 atm at 0°C	32 chips of X-ray CCD; 1 square inch, 1024x1024 pixels
X-ray energy range	2–20 keV	0.7–7 keV
Total detection area	5350 cm^2	200 cm^2
Energy resolution	18 % (5.9 keV)	$\leq 150 \text{ eV} (5.9 \text{ keV})$
Field of view*	1.5 x 160 degrees	1.5 x 90 degrees
Slit area for camera unit [†]	12.3 cm^2	1.35 cm^2
Detector position resolution	1 mm [‡]	0.025 mm (pixel size)
Localization accuracy	0.2 deg	0.2 deg
Absolute time resolution	50 μs	5.8 s
Weight	160 kg	11 kg

Notes.

- † GSC consists of 6 camera units. Each unit consists of two PCs. SSC consists of two camera units, SSC-Z and SSC-H. Effective area for one source is typically 6 cm 2 for one GSC camera when X-ray enters vertically to the detector. 1 cell width = 32 mm, with 3 beams shadows (1.4 mm width), and slit width 3.7 mm makes 6.1 cm 2 .
- ‡ For 8 keV at 1650 V. Most photons are softer than this, and many detectors were operated at 1550V to avoid spark. Observed position accuracy is the sum of this and slit width. It becomes 1.5 degrees or a little worse.

The transit time of a point source is 40–150 seconds with the FOV of 1.5° -width (FWHM) every 92-minute orbital period. Figure 3 illustrates the relation between the scan-transit time on each GSC counter and the source acquisition angle β from the rotation equator in the ISS normal attitude (see the geometry in figure 2). The scan duration increases from the ISS rotation equator ($\beta = 0^{\circ}$) towards the pole ($\beta = \pm 90^{\circ}$). Objects located along a great circle stay for 45 s in the FOV of MAXI cameras, where the time of stay is the shortest in the MAXI normal direction. For objects in the slanted field away from the great circle, the observation time becomes slightly longer.

Any target will come repeatedly in each field of the horizontal and zenithal cameras with every ISS orbital period. So in principle, a source is scanned twice in one orbit. But in fact, since the operation region is limited by the radiation zone, it is usually scanned only once in one orbit (Figure 5). As a matter of fact, MAXI coverage of the sky is as 80% in 1-orbit (92minutes) and 89% in 1-day.

The scanning direction and camera for a source changes with the 72 days cycle of ISS orbital precession. The sky near the scan poles comes out to the observable region in about two weeks. GSC is off when a part of the FOV of the camera comes at 5 degrees from the sun. However, the sum moves on the sky by 10 degrees in 10 days. Therefore there is no permanent invisible part of the sky. Because of these reasons the MAXI light curves often suffer a spurious 72-day oscillation.

^{*} FWHM \times Full-FOV.

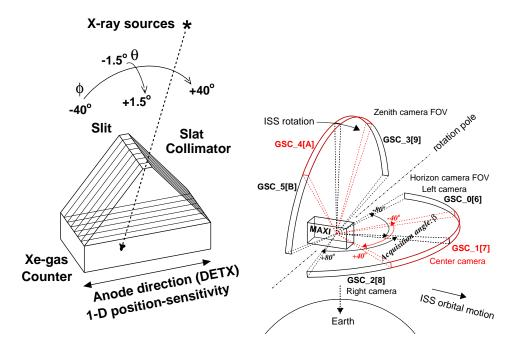


Fig. 2 Principle of MAXI Slit cameras. It consists of slit & slat collimators and one-dimensional position sensitive X-ray detector.

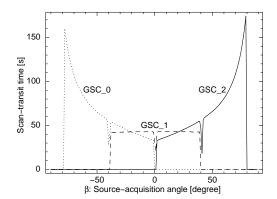
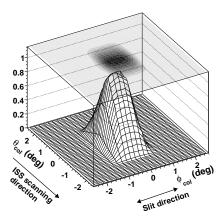


Fig. 3 Scan-transit time as a function of source-acquisition angle for each GSC unit of GSC_0, GSC_1, and GSC_2, in the ISS normal attitude.

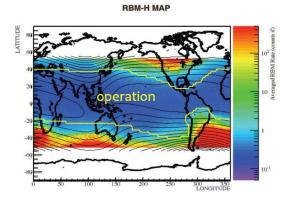
MAXI data will be down linked through the Low Rate Data Link (MIL1553B), and the Medium Rate Data Link (Ethernet). The basic data is contained in both rate data. MAXI is operated through the Operation Control System (OCS) at Tsukuba Space Center (TKSC), JAXA. MAXI data are processed and analyzed at TKSC, and also they are transferred to the Institute of Physical and Chemical Research (RIKEN). General users of MAXI can request the scientific data from RIKEN.

Fig. 4 Typical sample of PSF (Point Spread Function); a slat collimator has a triangular response (ISS scanning direction), while a slit and X-ray detector make a trapezoidal response. By monte-carlo simulation for incident angle 10 degrees and X=ray energy 5 keV for GSC.



This nova alert system has been developed to achieve automatic alert in section 4 ([6]). The MAXI team will also maintain archival data at RIKEN using the data from low-rate data and medium-rate data, such as all sky X-ray images, X-ray light curves of dedicated X-ray sources. In principle all astronomical data of MAXI will be available for public distribution ([7]). MAXI on-demand can process any part of the sky and any time in the mission ([29]).

Fig. 5 Count rates of Radiation belt monitor - Horizon (RBM-H) onboard MAXI. GSC is operated in the low background region, which is shown between the yellow lines. The MAP is set to MAXI and on/off of high voltage of GSC is automatically controlled.



2 GSC

The GSC is the main instrument of MAXI. We describe GSC by adopting explanation from [2].

The MAXI/GSC employs slit camera optics. The slit camera has an advantage of being free from the source contamination over the coded-aperture mask while it has a disadvantage in the limited slit area. To achieve the high sensitivity, large-area proportional counters filled with Xe gas are used for the X-ray detectors. The total detector area of $5350 \, \mathrm{cm}^2$ using twelve gas counters is optimized within the limit of the payload size $(0.8 \times 1.2 \times 1.8 \, \mathrm{m}^3)$.

Each set of six cameras is assembled into a module with the same FOV. One module points towards the direction of the ISS motion and the other towards the zenith. They are named as horizon and zenith modules, respectively. Each horizon/zenith module covers a wide rectangular FOV of $160^{\circ} \times 1.5^{\circ}$ (FWHM) with an almost equal geometrical area of 10 cm^2 . The 10° angle at the FOV edges on both the rotation poles are not covered because they are obstructed by the ISS structures.

The two FOVs of the horizon and the zenith modules would scan almost the entire sky in the 92 minutes orbital period if there were no high background region. In this case, any X-ray source is to be observed twice in one orbit. The horizon module scans first then followed by the zenith module after 21.5 minutes. The separation of the two FOV is 84°. Both FOVs have no Earth occultation and do not use any moving mechanics.

In the actual in-orbit operation, observation periods are limited in a low particle-background area in order to protect the counters from the heavy particle irradiation. It reduces the observation duty cycle down to $\sim 40\%$ [3]. The two FOVs are capable of covering the whole sky, although the scan frequency becomes once in an orbit.

2.1 Gas counter

The GSC proportional counters employ resistive carbon fibers with a diameter of $10 \, \mu m$ for anode wires. Higher resistive anodes are preferable for the better position resolution because the thermal noise on the readout signal is inversely proportional to the anode resistance. A carbon fiber is better than a nichrome wire. Although the traditional carbon-coated quartz has a larger resistance, it is mechanically weak, thus easy to break by launch vibration. The carbon fiber anodes in the GSC were developed at RIKEN and were successfully used in the HETE/WXM [8].

Figure 6 shows a picture of a single GSC proportional counter. All the flight counters were manufactured by Metorex (now a part of Oxford Instruments) in Finland. The front X-ray window has an area of 192×272 mm². It is sealed with a 100- μ m-thick beryllium foil. To support the pressure on the beryllium foil in vacuum that amounts 7300 N in the whole area, grid structures with a 17-mm height are placed every 10.6-mm pitch parallel to the anode wires. The vertical grid is placed only at the center to keep the open area as large as possible. The maximum pressure of 1.66 atm is expected at the temperature of 50° C. Every flight counter was tested to withstand 1.5 times higher than the design pressure, i.e. 2.5 atm. The bodies of the gas counters were made of titanium, which has sufficient strength and



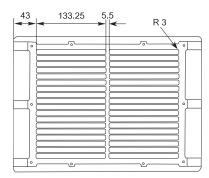


Fig. 6 Proportional counter used in GSC and drawing of the window from the top.

a heat expansion coefficient close enough to that of beryllium. The beryllium foil is glued on the body with epoxy.

Figure 7 shows the counter cross-section views. The gas cell is divided by ground wires into six carbon-anode cells for X-ray detection and ten tungsten-anode cells for particle veto. The carbon-anode layer and the bottom veto-detector layer have depths of 24 mm and 18 mm, respectively. These sizes are determined so that the main X-ray detectors and the veto detectors have enough efficiencies for X-rays in the 2–30 keV band and minimum-ionization particles, respectively. The minimum-ionization energy in the 18-mm thick Xe gas is 30 keV.

The carbon anodes and veto anodes are not located at the center of each cell in the vertical direction. The anode locations, the aspect ratios of these gas cells, and the spacings of the ground wires are determined so that the spatial non-uniformity of gas gain is small within each cell.

The tension of the carbon-anode wire is set to 4 gW, which is sufficiently smaller than the breakage limit, ~ 25 gW. All anode and ground wires are fixed via a spring at right end to absorb the difference of the heat expansion coefficient and keep the wires tight and straight. The veto anode wires are made of gold-coated tungsten with a 17- μ m diameter, which is pulled with a tension of 18 gW. We chose as thin wires as possible for veto anodes to achieve similarly high gas gain as the carbon anodes since the same high voltage (HV) is applied to both the carbon anodes and the veto anodes. The gas-gain ratio of carbon anode to the veto anode is 20:1. The ground wires are made of gold-coated tungsten with a 50 μ m diameter. Each tension is about 50 gW.

We tested several kinds of gas mixture and chose a combination of Xe (99%) + CO_2 (1%) with a pressure of 1.4 atm at 0°C. The amount of CO_2 is decreased from WXM PC (3%) [8] in order to reduce the spatial gas-gain non-uniformity, and still keep the sufficient quenching effect [9].

The position resolution and the energy resolution are incompatible requirements. The position resolution is primarily determined by the thermal noise on the resistive-anode wire against the readout signal charge. The higher gas gain is basically preferred for the better position resolution. However, the high voltage for the best

position resolution is usually in the limited proportionality region rather than the proportionality range, where the spatial gain non-uniformity is larger due to the space-charge effect, which also degrades the energy resolution. The operating high voltage (HV = 1650 V and the gas gain of 7,000) is chosen to achieve a sufficient position resolution and still keep an adequate energy resolution.

For the in-orbit calibration, a weak radioactive isotope of 55 Fe is installed in every counter, which illuminates a small spot of about 1 mm in diameter at the right end of the C2-anode cell (almost middle of the upper side in the left photo in Figure 6) Each isotope has a radiation of 30 kBq and its count rate by a GSC counter is about 0.2 c s^{-1} at the launch time.

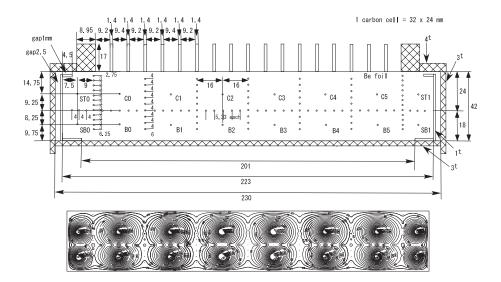


Fig. 7 Cross-section view of GSC proportional counter on the plane perpendicular to the anode wires. All anode/ground-wire locations are shown. The names for anode, C, B, ST and SB, denote Carbon, Bottom, Side Top and Side Bottom, respectively. The wires of B0 to B5 are connected together in the counter and read out as a single bottom-veto (BV) signal. The same for ST0, ST1, SB0 and SB1, as a side-veto (SV) signal. All numbers represent the scale in units of mm. Electric potential in the counter calculated by Garfield is shown in the below. The "Garfield" is a program to simulate gas counters developed in CERN (http://garfield.web.cern.ch/garfield/).

2.2 Electronics

Each GSC counter has six position-sensitive anodes readout at the both ends (left and right), and two signals for connected veto anodes. A total 14 preamplifiers are used for the 14 analog signals. We selected a hybrid-IC, Amptek A225, for the preamplifier, which is made with a space-use quality and has a low-power consumption. The

feedback capacities of veto anodes are left as they are 1 pF at the default, while those of carbon anodes are modified to 4 pF by adding an external 3 pF capacitor in order to obtain closer pulse heights for both signals from carbon anodes and veto anodes. The ratio becomes 5:1.

The maximum count rate in the current operation mode of MAXI is 40 Crab for a persistent source (lasting for the full scan length of 45 s), which is limited by the amount of event buffer and the 64 bit length of an event. Meanwhile, the maximum rate for the shorter time scale than 20 s is \sim 100 Crab, which is determined by the event transmission rate of the electronics.

2.3 Background in orbit

Figure 8 illustrates the background spectrum normalized by effective area, and those of the Ginga LAC ([10]) and the RXTE PCA ([11]), where expected contribution of the CXB in each instrument are included. Crab-like source spectra are shown together as the comparison. The GSC background is approximately 2 mCrab at 4 keV and 10 mCrab at 10 keV. The level is almost comparable to that of the Ginga LAC and slightly higher than that of the RXTE PCA.

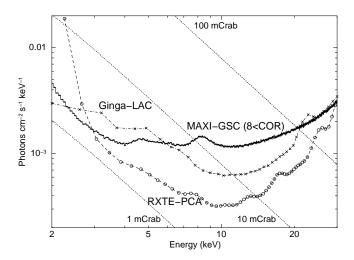


Fig. 8 GSC background energy spectrum normalized by effective area and comparison with those of Ginga-LAC, RXTE-PCA, and Crab-like source spectra. Expected contributions of the CXB in each instrument are included.

Figure 9 shows spatial distributions of the residual backgrounds along the anode wire in 2-10 and 10-30 keV energy bands and the estimated contributions of the CXB. Each GSC counter has a sensitivity gap at the center of the anode wire due to the frame structure to support 0.1-mm thick beryllium window. It causes the dip at

the center in the spatial distribution. The depth of the dips can be mostly explained by the extinction of the CXB component at the support structure.

The profile of the residual background left after subtracting the CXB component is primarily flat and slightly increases at both ends of the anode wires. It is because the efficiency of the anti-coincidence reduction decreases at the counter edge. The sensitivity is expected to get worse in these area.

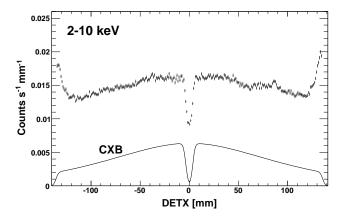


Fig. 9 Background spatial distribution in GSC gas counters along anode wires (DETX) in each energy band of 2-10 keV. Estimated contributions of the CXBs are shown with solid lines. The dips at the center (DETX=0) are due to the shadow of the support structure of the counter beryllium window.

Figure 2 in [12] is the background count rates in 4-10 keV band. The background rates sometimes went down to a half for some tens of days. These spans are when Soyuz spacecraft was not docked at the closest docking port. The gamma-ray altimeter of Soyuz spacecraft has a strong isotope (0.8 Ci of ¹³⁷Cs and ⁶⁰Co). It doubles the background of MAXI/GSC.

Figure 10 is the duty cycle (functioning time) of GSC. The average duty cycle of 40% comes from the limited operation on orbit where backgrounds by charged particles are low. At the time of 2020, two counters, camera 3, camera 6 are operated under the limited functionality (malfunctional veto counter).

On 2013 June 15, the gas gain of GSC camera 0 suddenly started to rise ([12] Figure 4). A small micrometeoride with about 50 μ m in diameter hit and cracked the Be window to cause a small gas leak. Since the gas leaked out, the operation of GSC camera 0 was stopped on 2020 August 15.

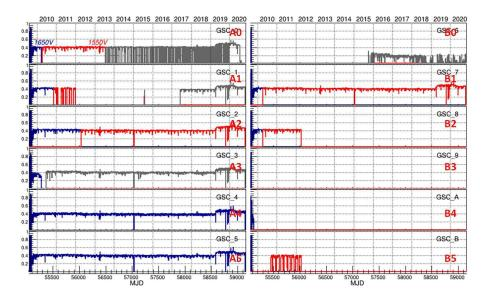


Fig. 10 Daily HV-on duty cycle of 12 GSC cameras from 2009 to 2020. Period of the standard operation with 1650 V is in blue, and 1550 V in and red lines. Those of the special condition is in gray lines.

3 SSC

3.1 X-ray CCD and its function

The SSC [4] consists of two identical SSC Units (SSCUs). They are thermally connected to an aluminum stand as shown in Fig. 11. Each SSCU consists of CCD units, preamplifiers, multiplexers, a collimator and slit unit, and a calibration source. The ISS orbits in a fixed orientation to the Earth so that MAXI always sees the sky. One SSCU (SSC-Z) monitors the zenithal direction and the other SSCU (SSC-H) monitors +20° above the horizontal direction. Each has 16 CCDs in 2×8 array, as shown in Fig. 11 [5]. Each CCD is a front-illuminated device, manufactured by *Hamamatsu Photonics* [13]. It is 25 mm square with a 24 μ m square pixel (1024 × 1024). Therefore, the geometrical area of the SSC (32 CCDs) is about 200 cm². An aluminum coating of 200 nm thickness on the CCD enables it to eliminate an optical blocking filter in front of the CCD, which in turn makes it possible to eliminate a vacuum tight body. The CCD is fabricated on an high-resistivity wafer, providing a thick depletion layer of about 70 μ m.

The SSC has no X-ray mirror, therefore the energy range of the SSC is determined by mainly CCD wafer. The quantum efficiency for soft X-ray is limited by absorption at the gate structure (dead layer) and aluminum coating on the front surface of the CCD wafer. That of hard X-ray is limited by the thickness of the depletion layer.

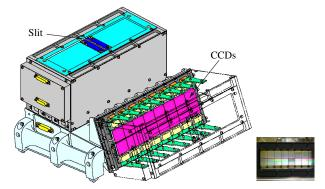


Fig. 11 Left is an exploded view of the SSC. Two SSCUs are set on the SSC stand. Right is a photograph of CCD array in an SSCU. The gap width between the adjacent CCDs is 0.4 mm.

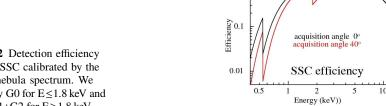


Fig. 12 Detection efficiency of the SSC calibrated by the Crab nebula spectrum. We employ G0 for E≤1.8 keV and G0+G1+G2 for $E \ge 1.8$ keV.

With taking into account the electronics, the effective energy range of the SSC is 0.5-12 keV. The SSCU has an entrance slit of 2.7 mm width just above the center of the CCD array that restricts the field of view (FOV) to 90°. Since the slit is just above the center of the camera, an acquisition angle of X-rays passing through the slit depends on the location of the CCD, resulting a different detection efficiency for each CCD. Fig. 12 shows the detection efficiency of the CCD by calibrating the Crab nebula [4]. We placed collimator sheets between the slit and the CCD array that restricts the FOV to 1.5. Since the slit and the collimator sheets are perpendicular to each other, we obtain the fan-beam FOV of the SSC, $90^{\circ} \times 1.5$. In this way, we run CCDs to function as one-dimensional imager. One orbit of the ISS covers 90° × 360°. The sky coverage region gradually shifts according to the precession of the ISS orbit. In this way, we can cover the entire sky about every 70-day.

The data handling scheme of the MAXI/SSC is similar to that of the previous satellites, which is given in the literature [5]. There is one video chain for each camera (16 CCDs) that runs CCDs in parallel sum mode where charges in multiple pixels are summed on-chip. In the standard operation, we obtain 16×1024 pixel data for each CCD. Since we sequentially read 16 CCD chips, the read-out time is 5.865 s that depends on the number of rows of the on-chip sum.

The inclination of the ISS orbit is 51%, resulting to pass at higher latitude regions than other X-ray missions in low-earth orbit. We switch off the bias level to the CCD during the passage of the South Atlantic anomaly (SAA) [14]. However, we keep switching on during the passage of high latitude region where the background is unstable and becomes too high to obtain good data. We employ event recognition method similar to the ASCA grade [16]. In the parallel sum mode, the charge spread of the signal is effectively valid only for G0 (single event), G1 (left split event), G2 (right split event) and G3 (three-pixel event). We do not see the charge spread in the vertical direction, therefore the background rejection efficiency is worse than that of the normal mode in other satellites. We expect that the X-ray events form G0, G1 or G2 while the charged particle event forms G3.

Furthermore, it degrades a performance of the CCD to pass through high particle background regions. The charged particles degrade the CCD performance by generating charge traps and by increasing dark current. Therefore, the CCD employed has two characteristics for radiation hardness. One is a notch structure that confines the charge transfer channel to a very narrow width. This actually improves the radiation-hardness by a factor of three [15]. The other is a charge-injection (CI) through which we can continuously inject some amount of charge at every 64 rows in the 64 binning mode [24]. The CI method can partly compensate for any degradation of the charge transfer inefficiency (CTI) of the CCD [17]. This technique [18] was, for the first time, added to the Suzaku XIS [19] in orbit and improved the performance of the CCD [20].

3.2 Cooling system

CCDs for X-ray detection in photon counting mode requires a low working temperature. The cooling system of the MAXI/SSC consists of two parts: one is a peltier device and the other is a radiator through a loop heat pipe (LHP). As shown in Fig. 13, the CCD chip (wafer and its silicon base) is mechanically supported by a single-stage peltier devices (24 posts made of bismuth telluride) so that we can cool the CCD chip. There are bonding wires between the CCD chip (cold part) and its surrounding hot part. Two SSCUs are placed on the SSC stand that is thermally connected to two radiator panels. One radiator panel (radiator-Z, 0.527m²) is facing to the zenith and the other (radiator-H, 0.357m²) is facing to the horizon. They are designed such that we can obtain the maximum area within the allocated volume of the MAXI. The radiator temperature depends on the day/night condition of the ISS. The LHP works as a heat-diode so that the colder radiator is selected to receive the heat from the SSC stand.

Fig. 14 shows the thermal history of the radiators and CCDs. The radiator-Z shows a large variation in day/night condition while the radiator-H shows a small variation. LHP functions properly and the body of the SSC is cooled around -20°C in orbit and is relatively stable. Therefore, we select to keep the peltier current constant rather

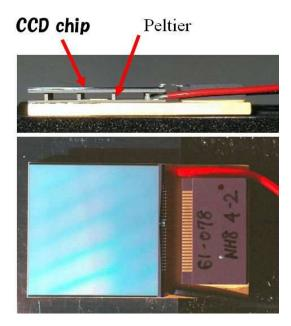


Fig. 13 Side view and top view of a CCD in the SSC.

than the CCD temperature constant [4]. The actual temperature of the CCDs are around -65°C that is well within the target temperature of -60°C.

In 2013, we had one CPU malfunctioned, that controlled the SSC-Z. It took about one year to recover. During this period, the SSC-Z stopped working and became the same temperature to that of the SSC stand. It is quite interesting to note that the temperature of the SSC-H increased in spite that the heat from the peltier devices became half. This can be understood that the LHP efficiency degraded due to the decrease of the heat input. After the recovery of the CPU, the thermal condition of the SSC also recovered as before.

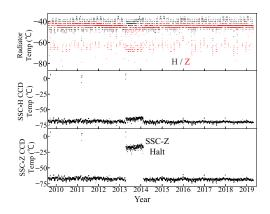


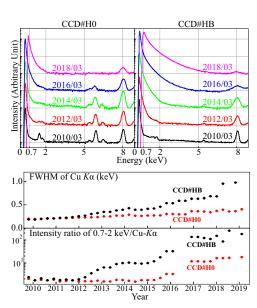
Fig. 14 Thermal history of the radiator-Z/H, CCDs in SSC-Z/H. CCD temperatures are relatively stable with an exception in 2013 when SSC-Z stopped working.

3.3 in orbit performance

The SSC functions properly during the night-time and detects X-ray events and particle events. However, it seriously suffers a signal overflows in the edge area of the CCD during the day time [4]. Sun light, particularly the infra-red, enters through the slit and is scattered inside the collimator. Therefore, we focus on the night-time observation. Furthermore, we can not obtain a useful data during the passage of the SAA and high background region. The effective observation efficiency is about 30%.

The increase of charge traps and dark current degrades SSC performance; a degradation of the energy resolution and an increase of the low energy background. The energy resolution can be monitored by characteristic X-rays. Radio-active sources of ⁵⁵Fe are installed at the edge of the SSCU. We also obtain continuous and uniform monitoring of Cu-K lines produced at the collimator by the incident particles. The low energy background can be monitored by the X-ray spectrum. Fig. 15 shows the spectral history of the two CCDs; one (CCD#HB) is at the center of the SSC and the other (CCD#H0) is at the edge of the SSC. The degradation of the CCD performance depends on the distance from the slit; CCD#HB receives higher flux of charged particle than CCD#H0. The FWHM of Mn-K was 147 eV and that of Cu-K was 170 eV at the time of launch [5]. A clear increase of the low energy is also noticed.

Fig. 15 Top panel shows the spectral evolution of CCD#H0 and CCD#HB. We can see a degradation of the emission line features of Cu-K α (8.09 keV) and Mn-K α (5.9 keV) as well as the increase at low energy. Bottom panel shows the degradation of the FWHM of Cu-K α and the intensity ratio between the low energy band (0.7-2 keV) and Cu-K α .



3.4 SSC all sky map

Point source catalog

There are two types of instruments to perform all-sky survey. One has a relatively narrow FOV; UHURU, Ariel V, HEAO I and ROSAT are of this type. They can take a long time to cover the entire sky, up to half a year in the case of ROSAT, while individual sources are observed for a relatively short period. As a result, they can miss sources that happen to be in quiet phase during its covering period. The other has a much wider FOV, like MAXI. It has a large fan beam FOV and scans the sky in every 92 minutes. Therefore, the source intensities listed in the MAXI catalog are accordingly the average ones over full survey period. Hence, MAXI is far less likely to miss sources that fall in quiescence for a relatively short period than the other type of all-sky survey.

MAXI/SSC has much lower sensitivity than that of MAXI/GSC whereas it can cover the energy range below 2 keV. The SSC source catalog [21], using the first 45-month data from 2010 August to 2014 April, contains two energy bands, 0.7-1.85 keV (soft) and 1.85-7.0 keV (hard). The limiting sensitivity of 3 and 4 mCrab are achieved and 140 and 138 sources are detected in the soft and hard energy bands, respectively. Combining the two energy bands, 170 sources are listed in the MAXI/SSC catalog. They are 22 galaxies including AGNs, 29 cluster of galaxies, 21 supernova remnants, 75 X-ray binaries, 8 stars, 5 isolated pulsars, 9 non-categorized objects and 2 unidentified objects. Comparing the soft-band sources with the ROSAT survey, which was performed about 20 years ago, 10% of the cataloged sources are found to have changed the flux since the ROSAT era.

Diffuse X-ray emission below 1 keV

SSC performed the all sky survey by using CCDs, particularly below 1 keV. After the background subtraction, we obtained the all sky maps in Fig. 16; the H-band

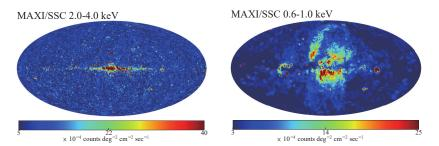


Fig. 16 Left is the SSC all sky map in the X-ray energy bands of 2.0-4.0 keV. Bright point sources are saturated in this color map so that a uniform background can be seen. Right is that in the X-ray energy bands of 0.7-1.0 keV. Various extended structures are seen.

(2-4 keV) map and the L-band (0.7-1.0 keV) map [22]. There are many point sources in H-band map while they are saturated so that we can see a uniform background as well as a galactic ridge emission. In the L-band map, we see many extended X-ray structures (EXSs); the Cygnus Super Bubble [23], the Vela SNR and a big one around the galactic center (GC). The L-band map is very similar to that obtained by ROSAT about 20 years ago.

In the diffuse X-ray background, the Solar Wind Charge eXchange (SWCX) is believed to play a major part, particularly at low energy since it was first noticed from comet observations by ROSAT [25]. It would affect the low energy (mainly below 1 keV) X-ray data with many emission lines. The intensity of the SWCX must correlate with the solar activity while it is not yet completely confirmed. The diffuse X-ray spectrum obtained by SSC can not be explained by the SWCX but by a thin thermal emission. They are relatively stable intensity during the SSC observation. The ROSAT observation was done near the peak of the solar cycle 22 while that of the SSC was done near the minimum at the beginning of the solar cycle 24. With taking into account these facts, we confirm that the diffuse X-ray emission at L-band is not generated by the SWCX but a celestial origin [22].

A large EXS is seen in the direction of the GC. There is some intensity inhomogeneity while they are thin thermal origin. We only constrain that the interstellar absorption feature is at least 0.6 times that of the galactic absorption feature. The brighter part of EXS is well within a circle of about 50° radius whose center is about 25° away from the GC. However, the distance to the EXS is not yet determined. If it is near the GC, a strong AGN activity is expected. If it is far from the galactic center and near-by, a hypernova or a series of supernova is plausible. A further observation is needed to understand its origin.

4 MAXI data flow and Nova Alert System

4.1 Data Flow

MAXI data are downloaded to NASA and transported to the JAXA Tsukuba Space Center (TKSC) in 5-6 seconds in total when the real-time contact is available [6]. About one-third of data are obtained during no real-time contact. They are once stored in the onboard data recorder, the High Rate Communication Outage Recorder (HCOR), in the ISS, and downloaded in the next contact one or two hours later.

Normal GSC event data and house-keeping (HK) data are downloaded through the robust low-rate ($\sim 25~kbps$) network with the Mil-1553B interface, and mainly used for transient event search and health checks of the detectors. Complete GSC and SSC event data and HK data are transmitted through the medium-rate network with the Ethernet interface whose maximum rate is 600 kbps.

The telemetry data are immediately processed at the TKSC, and stored into a PostgreSQL database in the MAXI photon-event database system (MAXI-DB) [26]. Different from other all-sky X-ray monitors with coded masks, the slit-camera

Table 2 Net 3- σ detection limits^a of the MAXI/GSC Nova-Alert System

Time bins	3-10 keV	2–4 keV	4–10 keV	10–20 keV
1 scan	60–100	80–120	80–120	400 ^b
4 orbits (~ 6 h)	25–30	50–70	30–50	200
1 days	12–15	25–30	15–20	100
4 days	7–8	15–20	8–10	50

^a The detection limits especially in shorter time bins depend on the number of detectors detected, incident angle, and background count rates. All the values are in unit of mCrab. ^b This and below limits are rough estimation.

design enables us to determine the direction of each incident X-ray, and store the data photon by photon. All the 1553B and Ethernet GSC, SSC, and HK data are provided from the ISAS/DARTS with the delay of about 1 hour and the NASA/HEASARC¹ for researchers to analyze the data. GSC light curves of more than 400 objects and the on-demnad analysis tool [29] are also available from the MAXI web site at RIKEN².

4.2 MAXI/GSC Nova-Alert System

The MAXI/GSC Nova-Alert System [6] is a system to find transient events promptly at the TKSC. The system consists of the *nova-search* system to search significant time variable events and the *alert* system to select events sent from the nova-search system and to issues alerts.

4.2.1 Nova-Search System

The nova-search system divides the celestial sphere into 49152 regions (pixels) with the same surface area of ~ 0.8 square degrees using the HEALPix C library [27]. The system receives 1553B GSC event data every second from the MAXI-DB, and accumulates the events into light curves at the corresponding celestial pixels. The time-bins and the energy-bands of the light curves investigated are 1-sec, 3-sec, 10-sec, 30-sec, 1-scan, 4-orbits, 1-day, and 4-days bins, and 3–10 keV, 2–4 keV, 4–10 keV, and 10–20 keV bands, respectively. Thus, the total number of the curves the system holds is $(49152 \text{ pixels} \times 8 \text{ time-scales} \times 4 \text{ energy-bands} =)1,572,864.$

Each light curve consists of ten time bins, nine of which are used to calculate average count rates. The rest of one and an additional one time bin are used to evaluate the latest count rates for real-time and delay-time (HCOR) data, respectively. The average count rate of the 1-scan bin data is also used as those of the short time (1–30 sec) bin data. Every second, the nova-search system calculates net exposure time,

b

¹ DARTS: https://www.darts.isas.jaxa.jp, HEASARC: https://heasarc.gsfc.nasa.gov

² http://maxi.riken.jp

effective area, and an expected background count rate in each pixel where X-rays enter. Using those information, trigger thresholds are calculated in all the time-scale bins. The criteria are given by chance probabilities typically less than or equal to $10^{-3\sim-4}$ for the background (and source count) fluctuation. Such low criteria result in a number of trigger events, ~ 1 events per second.

The nova-search system also play an important role as a real-time monitor developed by using the GTK+ library. The system gives us the real-time information about not only source activity but also detector health. The system produces all-sky images every 1-orbit, 4-orbits, 1-d, and 4-d, which are utilized for duty scientists to confirm and/or find transient events (not automatically triggered) by eye.

4.2.2 Alert System

The alert system accumulates the trigger events at the sky-map regions (pixels) sent from the nova-search system. The system issues alerts to the MAXI team (and the world for *burst* events) if the system receives trigger events at the adjoining two pixels without the interruption for more than 12 ks (>2 orbits), or the number of the triggers at one pixel containing a catalogued X-ray object exceeds 15 times. The first condition comes from the fact that a bright point source is expected to split into two or more pixels because the PSF of the GSC with the full-width at a half maximum of 1.5–2 deg is broader than the pixel size.

The system determines the source position from the triggered-count-weighted pixel-center coordinates of HEALPix for the multi-pixel events, and from the pixel-center coordinates for the single-pixel events. This and the positional insensitivity for the scan direction in the FOV within 1.5 degree make the position accuracy worse. The resultant 90% confidence error radius in the first E-mail alert is 0.7–0.8 arc-degree. The final localization for the alert is determined by fitting a source image with the point spread function of GSC cameras, resulting in an uncertainty of 0.3–0.4 arc-degree for less variable transient sources.

The system classifies detected (multi- or single-pixel) events into *Burst, Alert, Warning*, and *Info* events before sending E-mail notifications according to the significance, trigger timescales, and identification. For uncatalogued *Burst* events, the alert system automatically issues alerts to the world through the MAXI Mailing Lists and *The Gamma-ray Coordinates Network* (GCN) in 10–30 sec after the onboard detection. The duty scientists and senior staffs check all the events by eye, and, if necessary, manually issue alerts in tens of minutes to a few hours after the detection. The net $3-\sigma$ detection limits for transient events with the Nova-Alert system are summarized in Table 2.

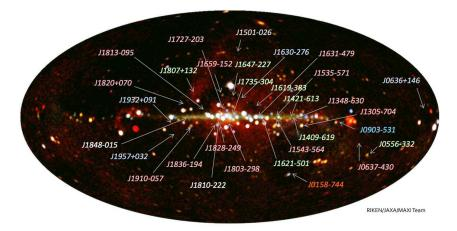


Fig. 17 31 X-ray novae MAXI newly discovered until the end of 2021. Black holes are shown in pink labels, neutron stars in green, probable neutron stars in light blue, a pulsar in blue, a white dwarf in red, and unknowns in white. The background image is the superposition of GSC and SSC false color images, obtained in the first 4.1 years and 3 years, respectively.

5 Scientific Highlights

The MAXI/GSC Nova-Alert system detected a number of transient events from short-term X/γ -ray burst events on time scales of seconds to long-term variabilities of X-ray binaries or AGNs on timescales of hours to days [6]. Some of them are soon reported to *The Astronomer's Telegram* (ATel) or GCN. We also report to GCN upper-limits of gravitational wave events by LIGO-Virgo and high energy neutrino events by ICE-Cube notified through GCN.

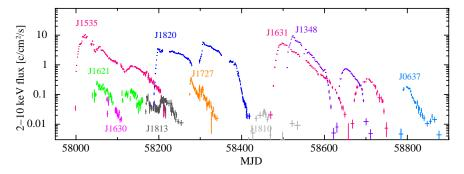


Fig. 18 2–10 keV light curves of MAXI novae observed from 2017 April 7 (MJD 57850) to 2020 February 21 (MJD 58900). Some curves at low count rates are truncated to avoid the complexity due to the overlaps. The count rate of the Crab nebula in the 2–10 keV band is 2.24 counts/cm²/s.

5.1 X-ray Bursts and Stellar Flares

On average, one X-ray burst was detected every week, and a few super- or long-burst every year. MAXI scanning observations every 92 min largely increased the number of the superbursts difficult to detect [30]. One bright stellar flare mainly from multiple systems, RS CVn stars and dMe stars, is also detected every month [33]. MAXI observed the upper ends for stellar flares with the luminosity of 10^{31-34} erg/s in the 2–20 keV band, leading to the discovery of a universal correlation of $\tau \propto L_{\rm X}^{0.2}$ between the flare duration τ and the intrinsic X-ray luminosity $L_{\rm X}$ in the 0.1–100 keV band.

5.2 X-ray Novae and Short-lived Transients

Until the end of 2021, MAXI newly discovered 31 X-ray novae or short-lived transients. Figure 17 displays positions of the new X-ray novae on the galactic coordinate; 14 black holes (candidates), 13 probable and confirmed neutron stars, 1 white dwarf, and 3 unknowns. After the discovery, except a few novae, precise localizations were performed mostly by J. Kennea and his collaborators with Swift/XRT in a few or several hours, sometimes, by NuSTAR or NICER.

Figure 18 shows examples of long-term light curves of MAXI X-ray novae. Continuous all-sky monitoring enables us to investigate detailed spectral evolution during the outbursts of these novae (e.g., [34] for J1535–571 and [35] for J1820+070). Peak fluxes of black hole X-ray novae range from several Crab to about 100 mCrab, and the fluxes at soft-to-hard transitions are also different by more than one order of magnitude. Taking account of the observational fact that the soft-to-hard transition occurs at a few percent of the Eddington luminosity [36], these implies that MAXI sees most black hole X-ray novae in the whole our galaxy [37].

MAXI also discovered short-lived transients lasting several hours or less, e.g., J1957+032 [38] and J0636-146. These are likely a kind of vary fast X-ray transient (VFXT). Peculiar short-term soft X-ray transients only seen below 4 keV were sometimes discovered. One of the unpredictable discoveries is MAXI J0158-744 found in the out-skirt of the Small Magellanic Cloud, the first discovery of an unusually massive O-Ne white dwarf close to, or possibly over, the Chandrasekhar limit with a companion Be star [40]. MAXI Unidentified Short Soft X-ray Transients (MUSSTs) are those which were detected only in one scan transit and no counterpart was found by prompt Swift/XRT followup observations. Such MUSST sources are not included to the above 31 new transients except for J1501-026 of highly significant detection. Recently one of the MUSSTs, GRB 140814A, is likely a merger-triggered core collapse supernova [39].

A few or several X-ray outbursts from known objects were also detected every year, e.g., V404 Cyg (GS 2023+338) and 4U 1730–22 appearing after 26 and 49 years, respectively. The recurrence periods of X-ray novae are also an important clue to know the number of compact stars in our Galaxy. In Table 3 the brightest X-ray

Table 3 The brightest X-ray transients above 1 Crab with MAXI in 2009-2021. In 2-20 keV in 1-day bin. They are transients backhole binaries or Be X-ray binaries.

name	F _X (Crab)	date
1 4U 1543-475	8.4	2021/6/15
2 Swift J0243.6+6124	8.2	2017/11/7
3 MAXI J1535-571	3.9	2017/9/20
4 A 0535+262	2.9	2020/11/23
5 MAXI J1348-630	2.6	2019/2/9
6 MAXI J1820+070	2.1	2018/7/6
7 MAXI J1631-479	1.3	2019/1/8
8 V 0332+53	1.0	2015/7/27
	1.0	

transient with MAXI are listed. This is in 2-20 keV and in 1-day bin. In the soft (2-4 keV) and hard (10-20 keV) bands, the rank changes. In the time-scale, the brightest persistent source is Sco X-1 (16 Crab) and the highest instant flux in the MAXI FOV was from SGR 1935+2154 (60 Crab in 0.2s on 2021/10/7).

5.3 Extragalactic Transients and MAXI Catalogs

MAXI detected about one *γ*-ray burst every month. *γ*-ray bursts MAXI detected tend to have soft energy spectra, suggesting those bursts are off-axis events [28]. The second bright flare from the first realtime observed tidal disruption event of a star by a massive black hole Swift J164449.3+573451 [31] was detected [32], which occurred about 34 hours after the first Swift/BAT detection. Longterm GSC monitoring observations of the whole sky allow us to detect 682 sources in the high Galactic latitude with fluxes down to 0.48 mCrab ($\simeq 5.9 \times 10^{-12}$ erg cm⁻² s⁻¹) in the 4–10 keV band [41], and 221 sources in the low Galactic latitude with fluxes down to 0.43 mCrab [42] in the first 7 years observations (2009/8 – 2016/7), which are published as the 3MAXI catalog (Figure 19). The flux level has almost reached the source confusion limit of GSC. 3MAXI catalogs are the new catalog in the 21st century, deepest in 4-10 keV band. They also provide precious long-term light curves of variable sources.

References

- Matsuoka, M. et al. PASJ 61 999 (2009) The MAXI Mission on the ISS: Science and Instruments for Monitoring All-Sky X-Ray Images
- 2. Mihara, T. et al. PASJ 63 S623 Gas Slit Camera (GSC) onboard MAXI on ISS
- 3. Sugizaki, M. et al. PASJ 63 S635 In-Orbit Performance of MAXI Gas Slit Camera (GSC) on
- Tsunemi, H. et al. PASJ 62 1371 (2010) In-Orbit Performance of the MAXI/SSC onboard the ISS

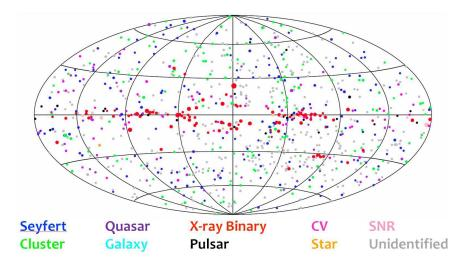


Fig. 19 3MAXI catalog in the early 21st century. Total 896 sources. [41], [42].

- 5. Tomida, H. et al. PASJ 63 397 (2011) Solid-State Slit Camera (SSC) Aboard MAXI
- Negoro, H. et al. PASJ 68 S1 (2016) The MAXI/GSC Nova-Alert System and results of its first 68 months
- Kohama, M. et al. proc. Astrophysics with All-Sky X-Ray Observations 40 (2009) MAXI data distribution and archive system
- 8. Shirasaki, Y. et al. PASJ 55 1033 (2003) Design and Performance of the Wide-Field X-Ray Monitor on Board the High-Energy Transient Explorer 2
- Mihara, T. et al. SPIE 4497 173 (2002) Performance of the GSC engineering counter for MAXI/ISS
- 10. Hayashida, K. et al. PASJ 41 373 (1989) The origin and behavior of the background in the large area counters on GINGA and its effect on the sensitivity
- 11. Jahoda, K. et al. ApJS 163 401 (2006) Calibration of the Rossi X-Ray Timing Explorer Proportional Counter Array
- 12. Mihara, T. et al. SPIE 9144 91441O (2014) MAXI: all-sky observation from the International Space Station
- 13. Tsunemi, H. et al. NIM-A 579 866 (2007) Development of a large format charge-coupled device (CCD) for applications in X-ray astronomy
- 14. Miyata, E. et, al. Japanese Journal of Applied Physics 42 4564 (2003) Proton Irradiation Experiment for X-ray Charge-Coupled Devices of the Monitor of All-Sky X-ray Image Mission Onboard the International Space Station: II. Degradation of Dark Current and Identification of Electron Trap Level
- 15. Tsunemi, H. et, al. IEEE Trans. 51 2288 (2004) Application of a Mesh Experiment for a Proton Beam Onto the Charge-Coupled Device
- Gendreau, K. C. PhD. thesis of Massachusetts Institute of Technology (1995) X-Ray Ccds for Space Applications: Calibration, Radiation Hardness, and Use for Measuring the Spectrum of the Cosmic X-Ray Background
- 17. Tomida, H. et al. PASJ 49 405 (1997) Radiation Damage on X-Ray CCDs and Restoration Technique for Space Astronomy
- Prigozhin, G. et al. IEEE Trans. 55 2111 (2008) CCD Charge Injection Structure at Very Small Signal Levels

- 19. Koyama, K. et al. PASJ 59 23 (2007) X-Ray Imaging Spectrometer (XIS) on Board Suzaku
- Uchiyama, H. et, al. PASJ 61 9 (2009) New CTI Correction Method for Spaced-Row Charge Injection of the Suzaku X-Ray Imaging Spectrometer
- Tomida, H. et, al. PASJ 68 S32 (2016) The first MAXI/SSC catalog of X-ray sources in 0.7-7.0 keV
- 22. Nakahira, S. et al. PASJ 72 17 (2020) MAXI/SSC all-sky maps from 0.7 keV to 4 keV
- 23. Kimura, M. et al. PASJ 65 14 (2013) Is the Cygnus Superbubble a Hypernova Remnant?
- 24. Miyata, E. et al. Japanese Journal of Applied Physics 41 7542 (2002) Proton Irradiation Experiment for X-ray Charge-Coupled Devices of the Monitor of All-Sky X-ray Image Mission Onboard the International Space Station: I. Experimental Setup and Measurement of the Charge Transfer Inefficiency
- Cravens, T. E. Geophys. Res. Lett. 24 105 (1997) Comet Hyakutake x-ray source: Charge transfer of solar wind heavy ions
- Negoro, H. et al. Astronomical Data Analysis Software and Systems (ADASS) XIII 314 452 (2004) MAXI Software System: Photon Event Database
- Górski, K. M. et al. ApJ 622 759 (2005) HEALPix: A Framework for High-Resolution Discretization and Fast Analysis of Data Distributed on the Sphere
- 28. Serino, M. et al. PASJ 66 87 (2014) MAXI observations of gamma-ray bursts
- Nakahira, S. et al. Journal of Space Science Informatics 2 29 (2013) Development of the MAXI/GSC all-sky data archive system
- 30. Serino, M. et al. PASJ 68 95 (2016) MAXI observations of long X-ray bursts
- 31. Burrows, D. N. et al. Nature 476 7361 (2011) Relativistic jet activity from the tidal disruption of a star by a massive black hole
- Kimura, M. et al. The Astronomer's Telegram 3244 1 MAXI/GSC observation of Swift J164449.3+573451
- Tsuboi, Y. et al. PASJ 68 90 (2016) Large X-ray flares on stars detected with MAXI/GSC: A
 universal correlation between the duration of a flare and its X-ray luminosity
- Nakahira, S. et al. PASJ 70 95 (2018) Discovery and state transitions of the new Galactic black hole candidate MAXI J1535-571
- Shidatsu, M. et al. ApJ 874 183 (2019) X-Ray and Optical Monitoring of State Transitions in MAXI J1820+070
- Vahdat M., et al. MNRAS 485 2744 (2019) Investigating state transition luminosities of Galactic black hole transients in the outburst decay
- Negoro, H. proc. 7 years of MAXI: monitoring X-ray Transients 15 (2017) Discovery of 17 X-ray Transients with MAXI/GSC and their Nature
- Beri, A. et al. MNRAS 486 1620 (2019) Unveiling the nature of compact object in the LMXB MAXI J1957+032 using Swift-XRT
- Dong, D. Z. et al. Science 373 1125 (2021) A transient radio source consistent with a mergertriggered core collapse supernova
- Morii, M. et al. ApJ 779 118 (2013) Extraordinary Luminous Soft X-Ray Transient MAXI J0158-744 as an Ignition of a Nova on a Very Massive O-Ne White Dwarf
- Kawamuro, T. et al. ApJS 238 32 (2018) The 7-year MAXI/GSC X-Ray Source Catalog in the High Galactic Latitude Sky (3MAXI)
- Hori, T. et al. ApJS 235 7 (2018) The 7-year MAXI/GSC Source Catalog of the Low-Galacticlatitude Sky (3MAXI)